This is an author's version published in: http://oatao.univ-toulouse.fr/21136

Official URL: https://doi.org/10.1016/j.electacta.2018.01.213

To cite this version:

Quaranta, D. and Massot, Laurent and Gibilaro, Mathieu and Mendes, Eric and Serp, Jérôme and Chamelot, Pierre
Zirconium(IV) electrochemical behavior in molten LiF-NaF. (2018) Electrochimica Acta, 265. 586-593. ISSN 0013-4686

Zirconium(IV) electrochemical behavior in molten LiF-NaF

D. Quaranta [a], L. Massot [b,*], M. Gibilaro [b], E. Mendes [a], J. Serp [a], P. Chamelot [b]

[a] *CEA Marcoule, Nuclear Energy Division, Research Department on Mining and Fuel Recycling Processes, SPDS/LDPS, Centre de Marcoule, BP 17171, 30207, Bagnols-sur-Cèze, France*
[b] *Laboratoire de Génie Chimique, Université de Toulouse, UPS, CNRS, INPT, 118 Route de Narbonne, 31062, Toulouse Cedex 9, France*

ABSTRACT

Zirconium has a large number of properties that make it very attractive for different applications in several activity fields (nuclear, pyrotechnics, armament …). This article is devoted to the study of zirconium electrochemical behavior and crystallization phenomena on silver electrode in the LiF-NaF eutectic mixture in the 690–900 °C temperature range, using cyclic voltammetry, square wave voltammetry and chronoamperometry. The result showed that Zr(IV) is reduced into Zr in a simple step exchanging four electrons and that zirconium nucleation is progressive whatever the temperature and the overvoltage. Nuclei growth takes place in all three dimensions and is limited by diffusion of Zr(IV) ions. The influence of overvoltage on the zirconium nucleation rate was also studied.

Keywords:
Zirconium
Electrochemistry
Progressive nucleation
Molten fluorides
Chronoamperometry

1. Introduction

Zirconium is a strategic metal used in various activity sectors because of its physicochemical properties: a low cross section of neutron capture, corrosion resistance under extreme conditions (high temperature, aggressive media), excellent mechanical resistance and high pyrophoricity [1]. 90% of the production of zirconium metal is used in the nuclear field, as zirconium alloy claddings (Zircaloy 2, Zircaloy 4, Zirlo …), U–Zr fuel, and dissolvers for spent fuel reprocessing [1,2]. Zirconium metal is also used in chemical engineering, pyrotechnics, armament, photography (flash lamps) and steel or other alloys formation [1]. Zirconium metal is obtained in the form of zirconium sponges produced by Kroll process [1,3]. The Kroll process consists in a reduction of zirconium chlorides to zirconium metal by magnesium acting as reducing metal.

Electrodeposition of zirconium in molten salts may be another process for production of zirconium metal [4,5]. Several studies on the electrochemical behavior of zirconium in molten chloride and fluoride media have been carried out [6–13]. In chloride media, results highlight the existence of several oxidation states (0, + I, + II and + IV). Zr(IV) reduction mechanism proposed by the authors diverge. Lee et al. [7] proposed a three step reduction mechanism whose redox couples are: Zr (IV)/Zr (II); Zr (II)/Zr and Zr(I)/Zr. Other authors showed a two step reduction mechanism whose redox couples differ [6,8,9]. For the first step, the authors agree on the reaction:

$\mathrm{Zr(IV)} + 2e^- \leftrightarrows \mathrm{Zr(II)}$ On the other hand, the second step of the reduction mechanism is more discussed and the proposed mechanisms are:

- $\mathrm{Zr(II)} + 2e^- \leftrightarrows \mathrm{Zr(0)}$ for Ghosh et al. [6].
- a combination of two reactions: $\mathrm{Zr(IV)} + 4e^- \leftrightarrows \mathrm{Zr(0)}$ and $\mathrm{Zr(IV)} + \mathrm{Cl}^- + 3e^- \leftrightarrows \mathrm{ZrCl}$ for Sakamura et al. [8].
- a combination of three reactions: $\mathrm{Zr(II)} + 2e^- \leftrightarrows \mathrm{Zr(0)}$, $\mathrm{Zr(IV)} + 4e^- \leftrightarrows \mathrm{Zr(0)}$ and $\mathrm{Zr(IV)} + \mathrm{Cl}^- + 3e^- \leftrightarrows \mathrm{ZrCl}$ for Fabian et al. [9].

In fluoride media, two different Zr (IV) ions reduction mechanisms have been proposed: either a two step reduction [12] or an one step reduction [10,11]:

$$\mathrm{Zr(IV)} + 2e^- \leftrightarrows \mathrm{Zr(II)} \qquad (1)$$

$$\mathrm{Zr(II)} + 2e^- \leftrightarrows \mathrm{Zr(0)} \qquad (2)$$

or

$$\mathrm{Zr(IV)} + 4e^- \leftrightarrows \mathrm{Zr(0)} \qquad (3)$$

---

* Corresponding author.
E-mail address: massot@chimie.ups-tlse.fr (L. Massot).

https://doi.org/10.1016/j.electacta.2018.01.213

The fundamental study of zirconium electrodeposition in molten fluorides is not described in the literature, particularly the nucleation and growth phenomena.

Present work focuses on the investigation of the electrochemical behavior of zirconium and the phenomena occurring at the beginning of electrolysis, by determining the Zr(IV) reduction mechanism using electroanalytical techniques. The second part of the study aims at determining the most suitable electrolytic process (DC electrolysis or pulsed current electrolysis) to obtain zirconium deposition. The phenomena of nucleation and crystal growth of zirconium on silver electrode in LiF–NaF were examined using chronoamperometry between 690 and 750 °C. Our experimental results are compared with the theoretical models corresponding to the two nucleation modes: progressive and instantaneous [14,15]. The influence of overvoltage and temperature on the nucleation mode and rate have also been examined in this work.

2. Experimental

2.1. Melt preparation

The electrolytic bath was composed of the LiF–NaF (Sigma Aldrich respectively ≥ 99.98% and 99.99%) eutectic mixture (60 40 mol%). The density (ρ/g.cm^{-3}) of this melt can be expressed as a function of the absolute temperature (T/K) by the following relation:

$$\rho \quad 2.5325{-}5.552.10^{-4}\,T \tag{4}$$

This mixture was initially dehydrated by heating under vacuum (7.10^{-5} bar) from ambient temperature up to its melting point (650 °C) for 70 h. After melting of the salt, pre electrolyzes were carried out using Ni cathode and glassy carbon anode in order to reduce residual oxide content. The anodic reaction consisted of carbon oxidation with oxide ions to form gaseous CO_2, which can be extracted out of the cell and consequently reduce oxide ions content in the melt. Pre electrolyzes were carried out until less than 1.1 × 10^{-3} mol kg^{-1} of oxide ions remain into the bath. This molality was determined by square wave voltammetry on gold electrode based on the work of L. Massot et al. [16]. Zirconium ions were added to the bath in the form of zirconium (IV) fluoride ZrF_4 (Alfa Aesar 99.9%).

2.2. Cell

Fig. 1 shows the electrochemical set up used in this study. The cell is composed of a vitreous carbon crucible placed in a boron nitride secondary crucible. The two crucibles were placed in a cylindrical reactor made of Inconel. It was closed by an Inconel lid cooled by air circulation. The experiments were carried out under an inert argon atmosphere (<0.1 ppm O_2 and <0.5 ppm H_2O). The cell was heated using a programmable furnace. The temperature was controlled by a platinum rhodium thermocouple. This equipment was placed in a glovebox under dry argon atmosphere (<15 ppm O_2 and < 2 ppm H_2O).

2.3. Electrodes

The working electrode was a sliver wire (1 mm diameter). The surface area of the working electrode was determined by measuring the immersion depth in the salt after each experiment. The counter electrode was a vitreous carbon (3000C) rod (3 mm diameter) with a large surface area. The potentials were referred to a platinum wire (1 mm diameter) immerged in the electrolytic bath. The platinum wire acts as a quasi reference electrode Pt/PtO$_x$/O^{2-} [17].

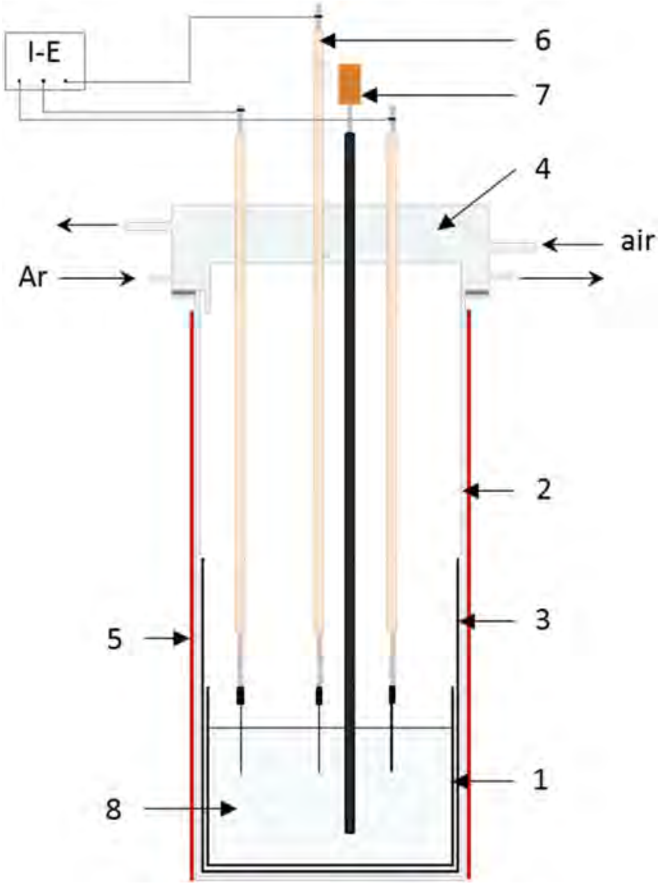

Fig. 1. The cell. (1) Vitreous carbon crucible; (2) Inconel chamber; (3) boron nitride liner; (4) air-cooled lid; (5) furnace; (6) electrodes; (7) thermocouple; (8) molten halide bath.

2.4. Techniques

Transient electrochemical techniques used for this study are cyclic voltammetry, square wave voltammetry and chronoamperometry. These investigations were carried out with a VSP potentiostat/galvanostat controlled with EC Lab V11.01 software.

3. Results and discussion

3.1. Zr(IV) ions reduction mechanism

3.1.1. Electrochemistry of Zr(IV) in LiF NaF

Cyclic voltammograms were plotted in the LiF NaF ZrF_4 (0.03–0.17 mol kg^{-1}) system between 750 and 900 °C on silver electrode at 100 mV s^{-1}. Fig. 2 shows a typical cyclic voltamogram of LiF NaF ZrF_4 (m_0 0.06 mol kg^{-1}) performed at 750 °C. This cyclic voltamogram shows a single reduction peak I_{Red} at around 0.99 V vs. Pt, associated with a reoxidation peak I_{Ox} at around 0.90 V vs. Pt. The shape of this peak is characteristic of the dissolution of soluble/insoluble system (stripping peak). The inset of Fig. 2 represents the variation of the peak current density and the peak potential versus the square root of the potential scan rate between 25 and 500 mV s^{-1}. The graph shows two important points: (i) the cathodic peak potential is independent of the scan rate, which is characteristic of a quasi reversible system, and (ii) there is a linear relationship between the cathodic peak intensity

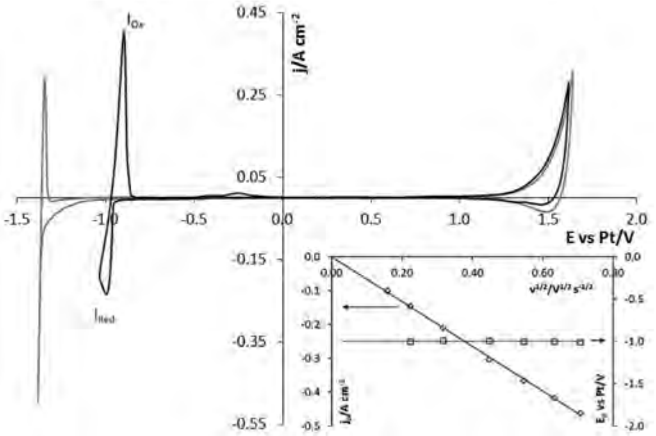

Fig. 2. Cyclic voltammograms on Ag of the LiF NaF system at 100 mV s ^{1} and 750 °C: without ZrF$_4$ (grey) and with ZrF$_4$ addition of 0.06 mol kg ^{1} (black). Inset. Variation of the peak current density (◊) and the peak potential (□) versus the square root of the potential scan rate. Working electrode: Ag (S 0.36 cm^2); auxiliary electrode: glassy carbon; comparison electrode: Pt.

and the square root of the scan rate. The reduction of Zr(IV) ions is thus controlled by the diffusion of Zr(IV) ions, and the Berzins Delahay relationship valid for a reversible soluble/insoluble system and a diffusion controlled reaction can be used [18]:

$$I_p \qquad 0.6102n\mathscr{F}Sc_0\left(\frac{n\mathscr{F}}{RT}\right)^{1/2}\mathscr{D}^{1/2}v^{1/2} \tag{5}$$

where I_p is the peak intensity (A), n the number of exchanged electrons, F the Faraday constant (96500 C mol^{-1}), S the electrode surface area (cm^2), c_0 the solute concentration (mol.cm^{-3}), R the gas constant (8.314 J mol^{-1}.K^{-1}), T the temperature (K), D the diffusion coefficient (cm^2. s^{-1}), v the scan rate (V.s^{-1}).

The slope of this linear equation for the LiF NaF ZrF$_4$ system (m_0 0.06 mol kg^{-1}) and at 750 °C is:

$$\frac{j_p}{v^{1/2}} \qquad 0.661A.s^{1/2}.cm^{-2}.V^{-1/2} \tag{6}$$

Fig. 3 represents the variation of the cathodic peak intensity as function of Zr concentration. Figure shows a linear dependency of the cathodic peak intensity with Zr concentration, confirming that this peak is attributed to the reduction of the Zr(IV) ions. The relationship between the intensity of the reduction peak and the Zr(IV) ion concentration is given at 750 °C:

$$j_p \qquad 3.11\,[Zr(IV)] \tag{7}$$

where j_p the peak current density, [Zr(IV)] the Zr(IV) molality (mol.kg^{-1}).

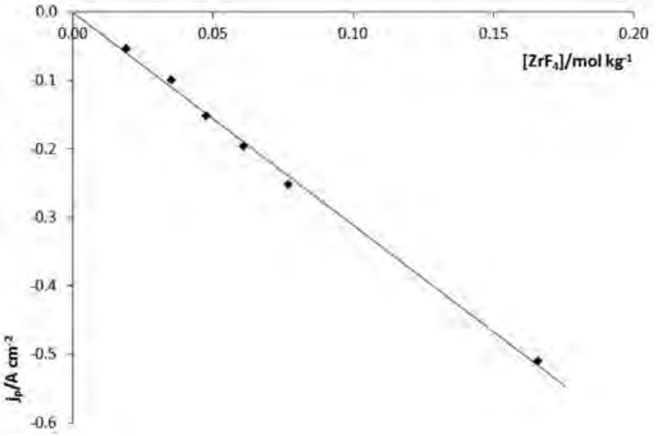

Fig. 3. Linear relationship between the cathodic peak current density and the ZrF$_4$ content in the bath in the LiF NaF system on Ag electrode at 100 mV s ^{1} and 750 °C.

3.1.2. *Number of exchanged electrons*

The electrochemical technique used to determine the number of exchanged electrons is the square wave voltammetry. In this technique, the applied potential is a combination of square and staircase signals. The two successive pulses of the square signal have the same amplitude, the same duration, but opposite signs [19]. In the case of a reversible soluble/soluble system, the square wave voltammetry curve is a Gaussian curve. The number of exchanged electrons is determined thanks to the half width of the peak, $W_{1/2}$, using the relationship [20]:

$$W_{1/2} \qquad 3.52\frac{RT}{n\mathscr{F}} \tag{8}$$

Fig. 4 shows a square wave voltamperogram of LiF NaF ZrF$_4$ (m_0 0.06 mol kg^{-1}) on silver electrode at 750 °C and 16 Hz. The voltamperogram shows a reduction peak at around 0.96 V vs Pt, which corresponds to the half wave potential $E_{p/2}$ of the cyclic voltammetry. The shape of the reduction peak is an asymmetric Gaussian, which is characteristic of a soluble/insoluble system [21]. The asymmetry of the peak is related to the irreversible crystallization phenomena leading to a nucleation overvoltage and therefore a delay in the occurrence of the faradic current [11,21,22].

Equation (8) can be applied as the linear relationship between the differential of the peak intensity and the square root of the frequency was verified in the 9–64 Hz frequency range in the inset of Fig. 4. The half width was determined as suggested by Hamel et al. [21] by doubling the value of the half width of the left side (2W$_L$) as in Fig. 4. Applying this method and Equation (8), the number of exchanged electrons has been determined and equal to 4.1 ± 0.1. The reduction of the Zr(IV) ions in LiF NaF is therefore carried out in a single step according to Equation (3).

Based on the work of Nourry et al. [23], square wave

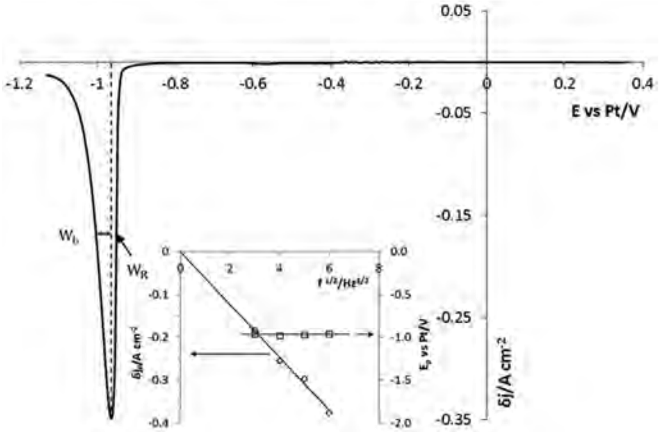

Fig. 4. Square wave voltammogram on Ag of the LiF NaF-ZrF$_4$ (m_0 0.06 mol kg ^{1}) at 16 Hz, pulse height: 20 mV, step potential: 2 mV and 750 °C. Inset. Variation of the differential of the peak current density (◊) and the peak potential (□) versus the square root of the frequency. Working electrode: Ag (S 0.35 cm^2); auxiliary electrode: glassy carbon; comparison electrode: Pt.

voltammetry can be used to determine the nucleation overvoltage η, using the following equation:

$$\eta \quad 2(W_L \quad W_R) \tag{9}$$

where W_L and W_R are respectively the half width of the left and the right side of the peak.

In our experiments, the overvoltage is equal to 50 mV.

3.1.3. *Diffusion coefficient determination*

The diffusion coefficient can be determined by two techniques: cyclic voltammetry and chronopotentiometry.

(i) Using the Berzins Delahay relationship (Equations (5) and (6)) and four exchanged electrons, Zr(IV) ions diffusion coefficient has been determined. The obtained value is 1.21×10^{-5} cm^2 s^{-1} at 750 °C in LiF NaF.

(ii) Chronopotentiometry was performed to confirm that the reduction of Zr (IV) ions is controlled by the diffusion of Zr (IV) ions. Fig. 5 shows a typical chronopotentiogram of LiF NaF ZrF_4 (m_0 0.06 mol kg^{-1}) on silver electrode at 750 °C and 40 mA. Several chronopotentiograms have been plotted for various intensities. As highlighted in the inset of Fig. 5, the product $I\tau^{1/2}$ vs. I is constant and in accordance with Sand's law [24]:

$$\frac{I\tau^{1/2}}{c_0} \quad 0.5n\mathscr{F}S(\pi\mathscr{D})^{1/2} \quad \text{constant} \tag{10}$$

where τ is the transition time (s).

The obtained value with the results of Fig. 5 for the LiF NaF ZrF_4 system (m_0 0.06 mol kg^{-1}) and 750 °C is:

$$\frac{j\tau^{1/2}}{c_0} \quad 1.257 \times 10^3 \text{A.s}^{1/2}\text{.cm.mol}^{-1} \tag{11}$$

Using equation (10), the diffusion coefficient has been determined and is equal to 1.35×10^{-5} cm^2 s^{-1} at 750 °C in LiF NaF, which is very close than the value obtained by cyclic voltammetry.

These values are in the same order of magnitude than Groult et al. (1,19.10^{-5} cm^2 s^{-1} at 694 °C) [10] and Xu et al. (1,13.10^{-5} cm^2 s^{-1} at 750 °C) [12] values.

The diffusion coefficient of Zr(IV) ions was calculated between 750 and 900 °C and the variation of the logarithm of the diffusion coefficient as a function of the inverse of the temperature is plotted in Fig. 6. The variation of Zr(IV) diffusion coefficient vs. $\left({}^{1}\!/_{T}\right)$ follows the Arrhenius type law expressed as:

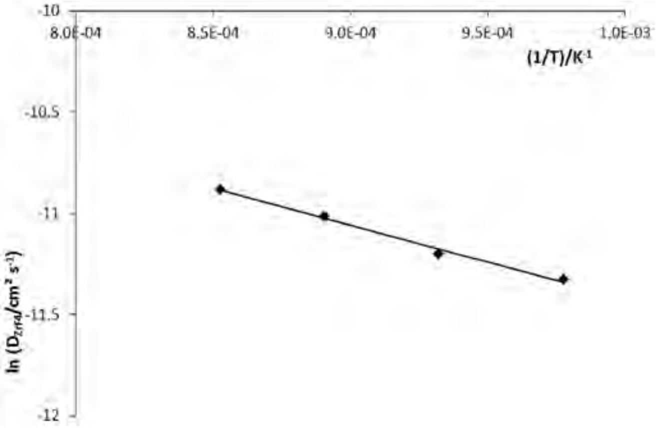

Fig. 6. Variation of the logarithm of the diffusion coefficient versus the inverse of the absolute temperature.

$$\mathscr{D}_{\text{Zr(IV)}} \quad \mathscr{D}^\circ \times exp\left(\frac{E_a}{RT}\right) \tag{12}$$

where $\mathscr{D}^\circ$ is the pre exponential factor (cm^2. s^{-1}) and E_a the activation energy (J.mol^{-1}).

Using results of Fig. 6, the following relationship is obtained:

$$\ln\mathscr{D}_{\text{Zr(IV)}} \quad 7.77 \quad \frac{3649}{T} \tag{13}$$

From the slope of Equation (12), the activation energy is equal to 30.3 kJ mol^{-1}.

3.2. *Zirconium electrocrystallisation process*

3.2.1. *Cyclic voltammetry*

Fig. 7 shows a cyclic voltammogram of LiF NaF ZrF_4 (m_0 0.17 mol kg^{-1}) on silver electrode at 710 °C. This cyclic voltammogram presents a cross over in the direct and reverse

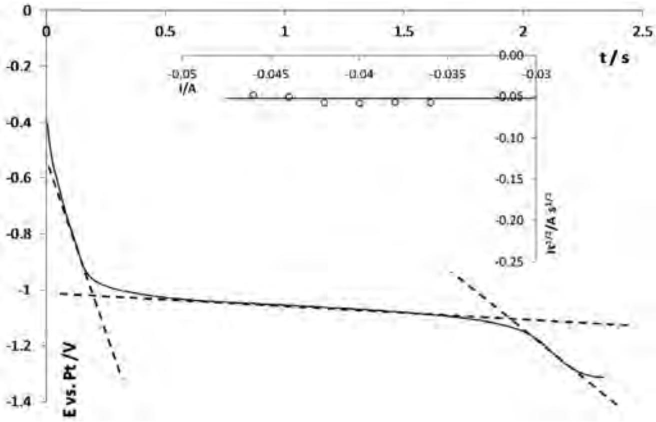

Fig. 5. Chronopotentiogram on silver electrode at −44 mA in LiF–NaF ZrF_4 (m_0 0.06 mol kg ^{1}) at 750 °C. Inset. Variation of $I\tau^{1/2}$ vs. the current at 750 °C. Working electrode: Ag (S 0.36 cm^2); auxiliary electrode: glassy carbon; comparison electrode: Pt.

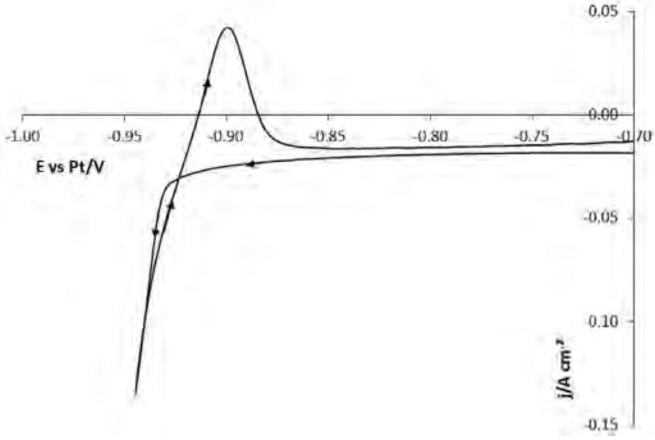

Fig. 7. Cyclic voltammogram illustrating the 'nucleation cross-over effect' on the reverse scan for zirconium deposition on a silver electrode in LiF–NaF–ZrF_4 (m_0 0.17 mol kg ^{1}) at 710 °C and 100 mV s ^{1}. Working electrode: Ag (S 0.36 cm^2); auxiliary electrode: glassy carbon; comparison electrode: Pt.

scanning. The cross over is assigned to the irreversibility of the nucleation step during the reduction scan [25], proving a solid phase formation which is zirconium metal.

3.2.2. Chronoamperometry

3.2.2.1. Determination of zirconium electrocrystallisation mode. Chronoamperometry is the electrochemical technique used in aqueous media, as well as in molten salts [14,15,25–28] to study the nucleation phenomena. The exploitation of the beginning of the graphs I f (t) gives information on the nucleation mode (instantaneous or progressive), the crystal growth mode and the geometry of the nuclei.

Fig. 8 illustrates a chronoamperogram obtained on silver electrode in LiF NaF $\mathrm{ZrF_4}$ (m_0 0.17 mol kg^{-1}) at 690 °C by imposing an overvoltage of 0.969 V vs. Pt. The curve is divided into three zones:

1. Part I is characterized by a sharp decrease in current, corresponding to the charge of the double layer and to the formation of the first germs. The germination's law giving the evolution of the number of nuclei as a function of time obeys the Poisson's law [15]:

$$N(t) \quad N_0\left(1 \quad e^{-At}\right) \tag{14}$$

where N is the growth center number at time t (cm^{-2}), N_0 the total number of favorable sites (cm^{-2}), A the germination rate constant (s^{-1}) and t the time (s).

   If the value of A is high, then N(t) N_0. Nucleation is instantaneous, meaning that all the zirconium nuclei form simultaneously.

   If the value of A is small, N(t) N_0At, the nucleation is then progressive. The nuclei are created continuously and therefore have different sizes.

2. Part II of the chronoamperogram shows a current increase, due to an increase of the electrode active surface area corresponding to the growth of the crystals. This zone presents a particular point where the rate of diffusion is equal to the crystal growth one. This point is the maximum of the peak and its coordinates are t_m and I_m. The analysis of Part II of the chronoamperogram provides information on the geometry of the nuclei, the nucleation mode and the phenomenon limiting crystal growth. Indeed, for very short times, the current intensity follows a relation of the type [15]:

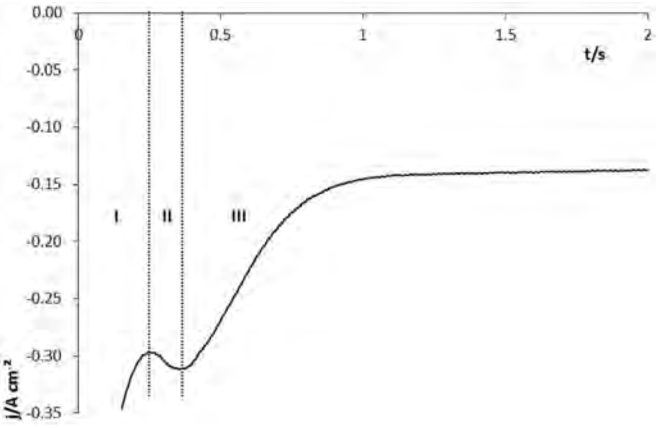

Fig. 8. Chronoamperogram on silver electrode at η −0.969 V vs Pt in LiF−NaF ZrF$_4$ (m_0 0.17 mol kg ^{1}) at 690 °C. Working electrode: Ag (S 0.35 cm^2); auxiliary electrode: glassy carbon; comparison electrode: Pt.

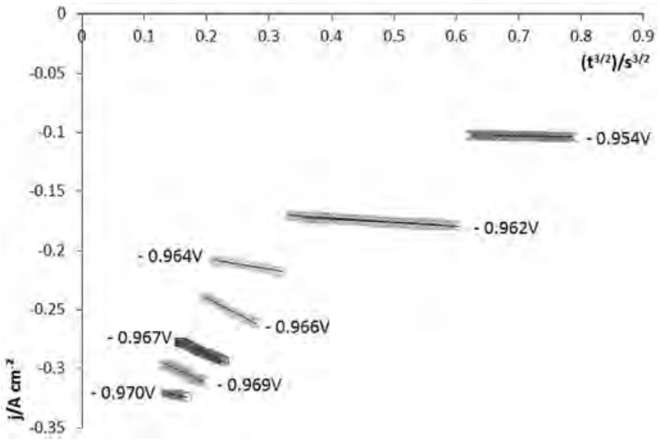

Fig. 9. Plotting of j f ($t^{3/2}$) of the chronoamperogram second part at various overvoltages (V vs Pt) in LiF NaF ZrF$_4$ (m_0 0.17 mol kg ^{1}) at 690 °C. Working electrode: Ag; auxiliary electrode: glassy carbon; comparison electrode: Pt.

$$j \quad \alpha t^x \tag{15}$$

where α and x depend on the nucleation mode, the nuclei geometry and the phenomenon limiting the growth of the crystals.

Considering hemispheric nuclei formation and three dimensional growth limited by diffusion, the parameter x is 1/2 for instantaneous nucleation and 3/2 for progressive nucleation [29]. Fig. 9 illustrates the relationship of proportionality between j and $t^{3/2}$. The nucleation of zirconium is therefore progressive and three dimensional. And the crystal growth is limited by the diffusion of Zr(IV) ions.

3. Part III shows a decrease in current intensity attributed to a limitation of the reaction by the diffusion phenomenon of Zr(IV) ions, according to Cottrell's law: I f ($t^{1/2}$) [30].

To confirm a progressive nucleation mode of zirconium, the experimental data were compared with the non dimensional theoretical models developed by Scharifker et al. [15]. These

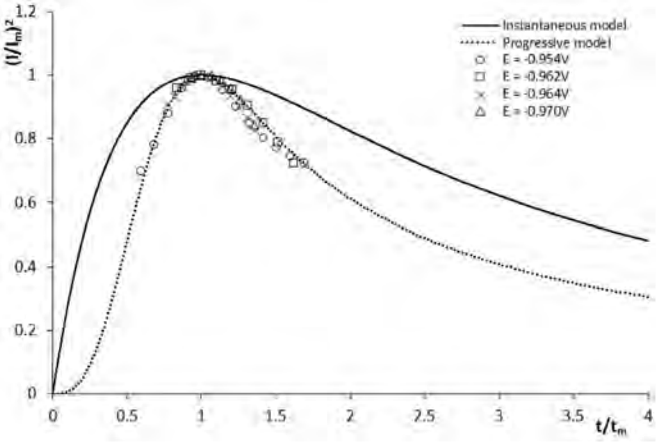

Fig. 10. Comparison of the dimensionless experimental data obtained from the current-time transients at various overvoltages with the theoretical models for instantaneous and progressive nucleation in LiF NaF ZrF$_4$ (m_0 0.17 mol kg ^{1}) at 690 °C. Working electrode: Ag; auxiliary electrode: glassy carbon; comparison electrode: Pt.

models give the expression of $\left(\frac{I}{I_m}\right)^2 \quad f\left(\frac{t}{t_m}\right)$ for the two nucleation modes. In the case of progressive nucleation, the non dimensional equation is the following:

$$\left(\frac{I}{I_m}\right)^2 \quad \frac{1.2254}{{}^{t}/{t_m}}\left(1 \quad e^{-2.3367\left(\frac{t}{t_m}\right)^2}\right)^2 \tag{16}$$

with

$$t_m \quad \left(\frac{4.6733}{AN_0\pi k'\mathscr{D}}\right)^{½}, \; k' \quad \frac{4}{3}\left[\frac{8\pi c_0 M}{\rho}\right]^{1/2} \tag{17}$$

$$j_m \quad 0.4615 n\mathscr{F}\mathscr{D}^{3/4}c_0\left(AN_0 k'\right)^{1/4} \tag{18}$$

and

$$j_m^2 t_m \quad 0.2598(n\mathscr{F}c_0)^2\mathscr{D} \tag{19}$$

where M the molar mass of Zr (g.mol^{-1}), ρ the density of Zr (g.cm^{-3}) and AN_0 the nucleation rate (cm^{-2}. s^{-1}).

Fig. 10 shows the experimental curves $\left(\frac{I}{I_m}\right)^2 \quad f\left(\frac{t}{t_m}\right)$ obtained from the chronoamerograms plotted on a silver electrode by imposing different overvoltages and the theoretical curves of the two nucleation modes. The influence of the temperature on the zirconium nucleation mode is illustrated in Fig. 11. Whatever the imposed overvoltage or the temperature of the salt bath, the experimental data fit the theoretical model of the progressive nucleation given by Equation (16).

In conclusion, the zirconium nucleation mode is progressive. The crystal growth takes place in three dimensions and is limited by the diffusion of the Zr(IV) ions on the surface of the electrode. The temperature and the overvoltage imposed on the electrode do not have any influence on the zirconium nucleation mode.

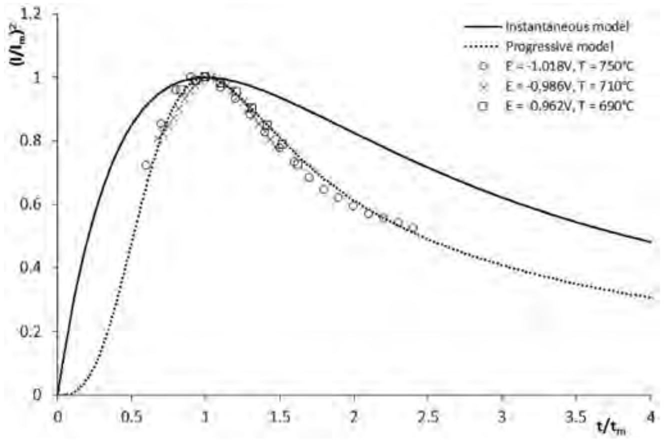

Fig. 11. Comparison of the dimensionless experimental data obtained from the current-time transients at various overvoltages and temperatures with the theoretical models for instantaneous and progressive nucleation in LiF NaF ZrF_4 (m_0 0.17 mol kg ^{1}). Working electrode: Ag; auxiliary electrode: glassy carbon; comparison electrode: Pt.

3.2.2.2. Determination of the nucleation rate AN_0. In the progressive nucleation mode, the nucleation rate, AN_0, can be determined for short electrolysis times and different overvoltages by coupling Equations (17) and (18). Values of the nucleation rate and of the product $I_m^2 t_m$ obtained at one temperature (690 °C) and one concentration of Zr(IV) ions (m_0 0.17 mol kg^{-1}) are gathered in Table 1. The nucleation rate increases with the increase of the overvoltage. The product $j_m^2 t_m$ is defined by Equation (19) for the progressive nucleation mode and by the following relation for the instantaneous nucleation mode:

$$j_m^2 t_m \quad 0.1629(n\mathscr{F}c_0)^2\mathscr{D} \tag{20}$$

In our experimental conditions, $j_m^2 t_m$ is equal to 4.0.10^{-2} A^2 s cm^{-4} in the case of a progressive nucleation and to 2.5.10^{-2} A^2 s cm^{-4} for an instantaneous nucleation. In our operating conditions, $I_m^2 t_m$ is approximately constant and the mean value of $j_m^2 t_m$ is (3.5 ± 0,9).10^{-2} A^2 s cm^{-4}, confirming that the nucleation of zirconium is progressive.

Fig. 12 shows a linear relation between ln (AN_0) and the inverse of the square of the overvoltage ($1/\eta^2$). Erdey Gruz and Volmer [31] showed that the nucleation rate obeys the following equation:

$$AN_0 \quad A_1 e^{-\frac{B_1}{\eta^2}} \tag{21}$$

This linearity observed in Fig. 12 is in agreement with Equation (20) and this expression is:

$$\ln(AN_0) \quad 110.1 \quad \frac{89.4}{\eta^2} \tag{22}$$

The nucleation rate, and therefore the nuclei formation, increase with the overvoltage.

3.3. First tests on zirconium electrodeposition

After the study of the zirconium electrocrystallization phenomena, first tests on zirconium electrodeposition were carried out in order to demonstrate the feasibility of obtaining zirconium metal deposits. Galvanostatic electrolyzes were performed at 0.03 A cm^{-2} during 5 h on graphite cathode in LiF NaF ZrF_4 (m_0 0.49 mol kg^{-1}) at 750 °C. Fig. 13a shows a photograph of the obtained deposit, where it can be noted that the coating is covered by cooled salt. However, some parts of the deposit are clearly visible and indicate a metallic dendritic structure. In order to confirm that metallic Zr was obtained, a cross section of the cathode was polished and characterized by SEM EDS analysis (see Fig. 13b). On this micrograph, the Zr coating is adherent and made of a dense layer (~10 μm of thickness) with some dendrites. The feasibility of metallic Zr electrodeposition is thus demonstrated.

4. Conclusion

The electrochemical behavior of ZrF_4 was investigated in LiF NaF eutectics between 750 and 900 °C on silver electrode. The reduction of ZrF_4 into metal occurs at around 0.99 V vs. Pt. Using different electroanalytical techniques, it was showed that:

the reduction of Zr(IV) takes place in a single step exchanging 4 electrons:
$Zr(IV) + 4e^- \leftrightarrows Zr(0)$,
the reduction is controlled by diffusion of Zr(IV) ions.

The diffusion coefficient of Zr(IV) ions was obtained on a temperature range from 750 to 900 °C. The data show an Arrhenius type relationship between the logarithm of the diffusion coefficient and the inverse of the temperature.

Then, zirconium crystallization was investigated in a LiF NaF salt

Table 1
Influence of the overvoltage on the nuclei density in LiF–NaF–ZrF_4 ($\mathbf{m}_0$ = 0.17 mol kg^{-1}) at 690 °C. Working electrode: Ag; auxiliary electrode: glassy carbon; comparison electrode: Pt.

η (V vs Pt)	t_m (s)	j_m (A.cm^{-2})	S (cm^2)	10^3 $I_m^2.t_m$ (A^2.s)	10^{-5} AN_0 (cm^{-2}.s^{-1})
−0.954	1.55	−0.127	0.283	2.00	1.42
−0.962	0.693	−0.178	0.346	2.61	7.14
−0.962	0.716	−0.179	0.346	2.72	6.69
−0.964	0.520	−0.221	0.346	3.03	12.7
−0.966	0.487	−0.270	0.314	3.50	14.5
−0.967	0.405	−0.297	0.314	3.54	20.9
−0.969	0.355	−0.312	0.314	3.40	27.2
−0.970	0.309	−0.324	0.346	3.87	36.0

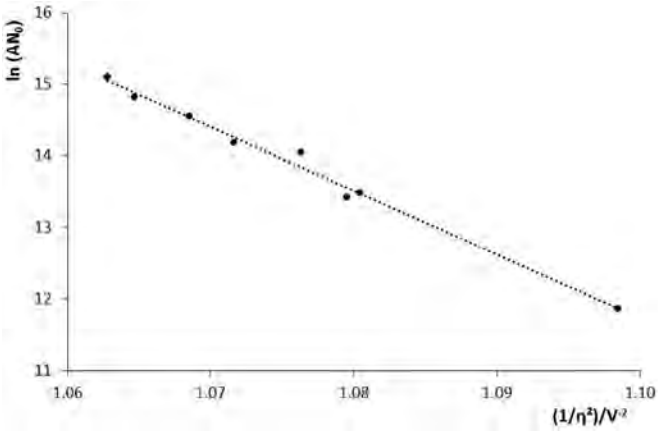

Fig. 12. Linear relationship between the logarithm of the nuclei density and the inverse square overvoltage in LiF–NaF–ZrF_4 (m_0 = 0.17 mol kg^{-1}) at 690 °C. Working electrode: Ag; auxiliary electrode: glassy carbon; comparison electrode: Pt.

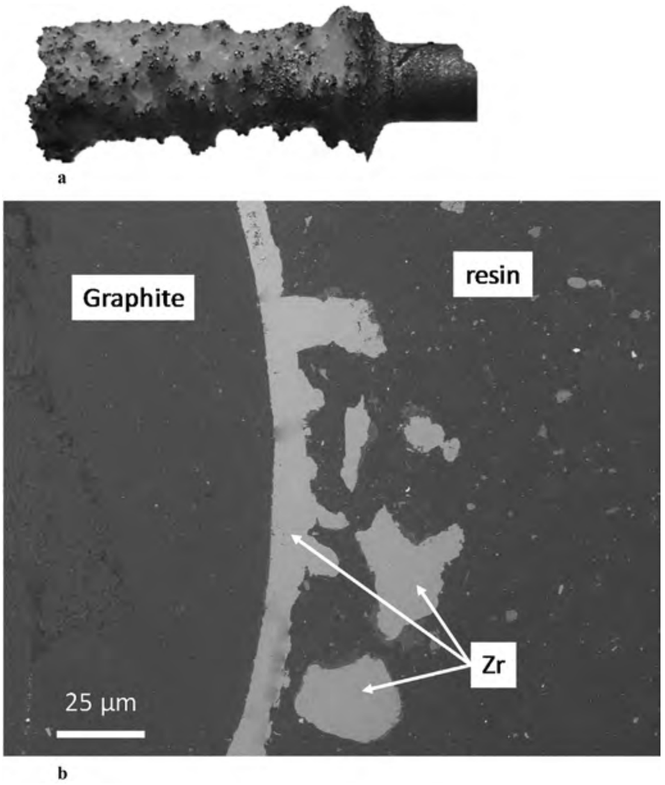

Fig. 13. a and b: Photograph (a) and SEM micrograph of the cross section (b) of Zr deposit on graphite cathode after electrolysis in LiF-NaF-ZrF_4 (m_0 = 0.49 mol kg^{-1}) at 750 °C; i = −0.03 A cm^{-2}; t = 5 h.

mixture on silver electrode using chronoamperometry. In these conditions, zirconium nucleation was demonstrated to be progressive, which means that the nuclei are formed continuously. In addition, the shape of zirconium nuclei is hemispherical. Their growth is achieved in the three dimensions and is limited by the diffusion of Zr(IV) ions. Finally, the temperature and the overvoltage do not have any influence on the zirconium nucleation mode, which remains progressive. However, the overvoltage influences the nucleation rate: the increase in the overvoltage generates an increase in the number of nuclei formed.

These results are important and provide information on the deposition strategy. Indeed, the nucleation is progressive, DC electrolysis appears to be suitable for zirconium deposition. With a progressive nucleation model, it is preferable to have a high temperature, a high concentration and an high enough overvoltage to make a deposit having the best conditions [27]. First experiments were performed on graphite cathode in order to demonstrate the feasibility of metallic Zr electrodeposition in molten fluoride media. The influence of the operating parameters on the electroplating of zirconium (concentration, temperature, cathodic substrate, applied intensity) are under investigation and the results will be detailed in a future article.

References

[1] R. Tricot, Zirconium et hafnium, Tech. Ing., 1994.

[2] P. Bihouix, B.D. Guillebon, Quel futur pour les métaux? Raréfaction des métaux: un nouveau défi pour la société, EDP Sciences, 2013.

[3] B. Lustman, F. Kerze, The Metallurgy of Zirconium, McGraw-Hill, 1955.

[4] G.J. Kipouros, S.N. Flengas, Electrorefining of zirconium metal in alkali chloride and alkali fluoride fused electrolytes, J. Electrochem. Soc. 132 (1985) 1087–1098.

[5] H. Groult, A. Barhoun, E. Briot, F. Lantelme, C.M. Julien, Electrodeposition of Zr on graphite in molten fluorides, J. Fluorine Chem. 132 (2011) 1122–1126.

[6] S. Ghosh, S. Vandarkuzhali, P. Venkatesh, G. Seenivasan, T. Subramanian, B. Prabhakara Reddy, K. Nagarajan, Electrochemical studies on the redox behaviour of zirconium in molten LiCl–KCl eutectic, J. Electroanal. Chem. 627 (2009) 15–27.

[7] C.H. Lee, K.H. Kang, M.K. Jeon, C.M. Heo, Y.L. Lee, Electrorefining of zirconium from Zircaloy-4 cladding hulls in LiCl-KCl molten salts, J. Electrochem. Soc. 159 (2012) D463–D468.

[8] Y. Sakamura, Zirconium behavior in molten LiCl-KCl eutectic, J. Electrochem. Soc. 151 (2004) C187–C193.

[9] C.P. Fabian, V. Luca, T.H. Le, A.M. Bond, P. Chamelot, L. Massot, C. Caravaca, T.L. Hanley, G.R. Lumpkin, Cyclic voltammetric experiment - simulation comparisons of the complex mechanism associated with electrochemical reduction of Zr^{4+} in LiCl-KCl eutectic molten salt, J. Electrochem. Soc. 160 (2013) H81–H86.

[10] H. Groult, A. Barhoun, H.E. Ghallali, S. Borensztjan, F. Lantelme, Study of the electrochemical reduction of Zr^{4+} ions in molten alkali fluorides, J. Electrochem. Soc. 155 (2008) E19–E25.

[11] M. Gibilaro, L. Massot, P. Chamelot, L. Cassayre, P. Taxil, Investigation of Zr(IV) in LiF–CaF_2: stability with oxide ions and electroreduction pathway on inert and reactive electrodes, Electrochim. Acta 95 (2013) 185–191.

[12] L. Xu, Y. Xiao, Q. Xu, A. van Sandwijk, Z. Zhao, Q. Song, Y. Cai, Y. Yang, Electrochemical studies on the redox behavior of zirconium in the LiF-NaF eutectic melt, J. Nucl. Mater. 488 (2017) 295–301, https://doi.org/10.1016/j.jnucmat.2017.03.028.

[13] L. Xu, Y. Xiao, Q. Xu, A. van Sandwijk, J. Li, Z. Zhao, Q. Song, Y. Yang, Electrochemical behavior of zirconium in molten LiF–KF–ZrF_4 at 600 °C, RSC Adv.

6 (2016) 84472 84479.

[14] G. Gunawardena, G. Hills, I. Montenegro, B. Scharifker, Electrochemical nucleation - Part I general considerations, J. Electroanal. Chem. Interfacial Electrochem. 138 (1982) 225 239.

[15] B. Scharifker, G. Hills, Theoretical and experimental studies of multiple nucleation, Electrochim. Acta 28 (1983) 879 889.

[16] L. Massot, L. Cassayre, P. Chamelot, P. Taxil, On the use of electrochemical techniques to monitor free oxide content in molten fluoride media, J. Electroanal. Chem. 606 (2007) 17 23. http://www.sciencedirect.com/science/article/pii/S0022072807001994. (Accessed 18 March 2016).

[17] A.D. Graves, D. Inman, Adsorption and the differential capacitance of the electrical double-layer at platinum/halide metal interfaces, Nature 208 (1965) 481 482, https://doi.org/10.1038/208481b0.

[18] T. Berzins, P. Delahay, Oscillographic polarographic waves for the reversible deposition of metals on solid electrodes, J. Am. Chem. Soc. 75 (1953) 555 559.

[19] L. Ramaley, M. Krause, Theory of square wave voltammetry, Anal. Chem. 41 (1969) 1362, https://doi.org/10.1021/ac60280a005.

[20] P. Chamelot, B. Lafage, P. Taxil, Using square-wave voltammetry to monitor molten alkaline fluoride baths for electrodeposition of niobium, Electrochim. Acta 43 (1998) 607 616, https://doi.org/10.1016/S0013-4686(97)00102-3.

[21] C. Hamel, P. Chamelot, A. Laplace, E. Walle, O. Dugne, P. Taxil, Reduction process of uranium(IV) and uranium(III) in molten fluorides, Electrochim. Acta 52 (2007) 3995 4003.

[22] C. Hamel, P. Chamelot, P. Taxil, Neodymium(III) cathodic processes in molten fluorides, Electrochim. Acta 49 (2004) 4467 4476, https://doi.org/10.1016/j.electacta.2004.05.003.

[23] C. Nourry, L. Massot, P. Chamelot, P. Taxil, Data acquisition in thermodynamic and electrochemical reduction in a Gd(III)/Gd system in LiF CaF2 media, Electrochim. Acta 53 (2008) 2650 2655, https://doi.org/10.1016/j.electacta.2007.10.050.

[24] R.K. Jain, H.C. Gaur, B.J. Welch, Chronopotentiometry: a review of theoretical principles, J. Electroanal. Chem. Interfacial Electrochem. 79 (1977) 211 236, https://doi.org/10.1016/S0022-0728(77)80444-0.

[25] L. Legrand, A. Tranchant, R. Messina, Electrodeposition studies of aluminum on tungsten electrode from $DMSO_2$ electrolytes determination of Al^{III} species diffusion coefficients, J. Electrochem. Soc. 141 (1994) 378 382.

[26] P. Chamelot, B. Lafage, P. Taxil, Studies of niobium electrocrystallization phenomena in molten fluorides, J. Electrochem. Soc. 143 (1996) 1570 1576.

[27] L. Massot, P. Chamelot, P. Palau, P. Taxil, Electrocrystallisation of tantalum in molten fluoride media, Electrochim. Acta 50 (2005) 5408 5413.

[28] A.L. Bieber, L. Massot, M. Gibilaro, L. Cassayre, P. Taxil, P. Chamelot, Silicon electrodeposition in molten fluorides, Electrochim. Acta 62 (2012) 282 289.

[29] P. Allongue, E. Souteyrand, Metal electrodeposition on semiconductors: Part I. Comparison with glassy carbon in the case of platinum deposition, J. Electroanal. Chem. Interfacial Electrochem. 286 (1990) 217 237.

[30] A.J. Bard, L.R. Faulkner, Electrochimie: principes, méthodes et applications, Masson, 1983.

[31] T. Erdey-Grúz, M. Volmer, Zur Frage der elektrolytischen Metallüberspannung, Z. Für Phys. Chem. 157A (1931) 165 181.